Full-Process Operation, Control, and Experiments of Modular High-Frequency-Link DC Transformer Based on Dual Active Bridge for Flexible MVDC Distribution: A Practical Tutorial

Biao Zhao, *Member, IEEE*, Qiang Song, *Member, IEEE*, Jianguo Li, Qianhao Sun, and Wenhua Liu

***Abstract*—DC transformer (DCT) will be the key device for medium-voltage dc (MVDC) power distribution system. This paper gives a practical tutorial on full-process operation, control, and experiments for application of DCT based on dual active bridge in flexible MVDC distribution system. The operation of DCT for MVDC distribution is designed to three modes: MVDC, low-voltage dc (LVDC), and power control modes. Three optimal modulation methods during startup, steady, and transient processes are proposed which can reduce current impact in practice. A full-process control strategy during operation state is proposed to achieve flexible control and fast management of voltage and power in MVDC distribution system, especially an optimal balance control during block process is proposed to reduce power losses. On this basis, a fault-handling solution is proposed to improve reliability of DCT in practice, and a hardware design method is proposed to enhance flexibility and modularity. Finally, an industrial prototype is built, and comprehensive experiments verify the validity and effectiveness of the proposed solution. The practical application of DCT in MVDC distribution are expected, and the exploration of this study could provide valuable references for the practical DCT design.**

***Index Terms*—DC microgrid, dc power distribution, dc transformer (DCT), dc transmission, dual active bridge, high-frequency (HF) link, medium-voltage dc (MVDC), solid-state transformer.**

I. Introduction

COMPARED with dc power transmission, dc power distribution is gradually attracting the attention of researchers in recent years. However, many concepts are still in the exploratory stage [1], [2]. In dc power distribution, most of studies focuses on low-voltage dc (LVDC) microgrid, and the medium-voltage distribution grid usually focuses on the ac grid [3]–[7]. To date, flexible HVDC (VSC-HVDC) transmission is being rapidly developed, turning medium-voltage dc (MVDC) distribution network into a reality [8]–[10]. In this context, dc for MVDC distribution will further promote the development of HVDC transmission and LVDC microgrid, eventually resulting in considerable amount of technical advantages.

Fig. 1 shows a demonstration scheme for flexible MVDC power distribution system in China. The application directions of the project are centered on the following: 1) improving the reliability of power supply; 2) improving power quality; 3) interaction of distributed generation and storage battery; and 4) interface of sensitive ac loads and dc loads. A dc transformer (DCT) is necessary to achieve voltage conversion, flexible power management, and electrical isolation between MVDC distribution bus and LVDC microgrid bus [11], [12].

In reality, realizing power conversion in MVDC distribution through the use of simple magnetic transformer, which is widely used in ac distribution, is difficult [13]; it especially requires power electronics technology. In LV applications, dc–dc converters are widely used. Moreover, many literatures discussed isolated bidirectional dc–dc converters (IBDCs), which are very important in achieving electrical isolation [14]–[20]. These converters can be used to access dc loads, energy storage systems, and distributed generations in dc microgrids. However, these converters fail to serve as permanent interfaces between MVDC distribution bus and LVDC microgrid.

Moreover, many literatures have investigated various multiple dc–dc converters to increase voltage/power level [21]–[23], but primarily focusing on unidirectional dc–dc converters. The target objects are usually buck/boost circuits or isolated dc–dc converters (the input bridge is an active-controlled inverter and output bridge is a noncontrolled rectifier), and the output voltage of these converters is controlled by the duty ratio of switches. These types of dc converters cannot meet the application requirements of DCT in flexible MVDC distribution, such as bidirectional power flow, electrical isolation, high-power application, etc.

On this basis, some literatures also discussed multiple IBDCs [24], [25]. Three existing IBDC topologies, dual-half-bridge, dual-active-bridge (DAB), and series resonant converters were analyzed and compared [24]. Owing to its advantages, such

Manuscript received April 6, 2016; revised June 22, 2016 and September 5, 2016; accepted November 1, 2016. Date of publication November 14, 2016; date of current version April 24, 2017. This work was supported by the National Natural Science Foundation of China under Grant 51507089. Recommended for publication by Associate Editor M. Ordonez. *(Corresponding author: Qiang Song.)*

B. Zhao, Q. Song, Q. Sun, and W. Liu are with the Department of Electrical Engineering, Tsinghua University, Beijing 100084, China (e-mail: zhaobiao112904829@126.com; songqiang@tsinghua.edu.cn; sxsunqianhao@163.com; liuwenh@tsinghua.edu.cn).

J. Li is with the North China Electric Power University, Beijing 102206, China (e-mail: lijianguo@tsinghua.edu.cn).

Color versions of one or more of the figures in this paper are available online at http://ieeexplore.ieee.org.

Digital Object Identifier 10.1109/TPEL.2016.2626262

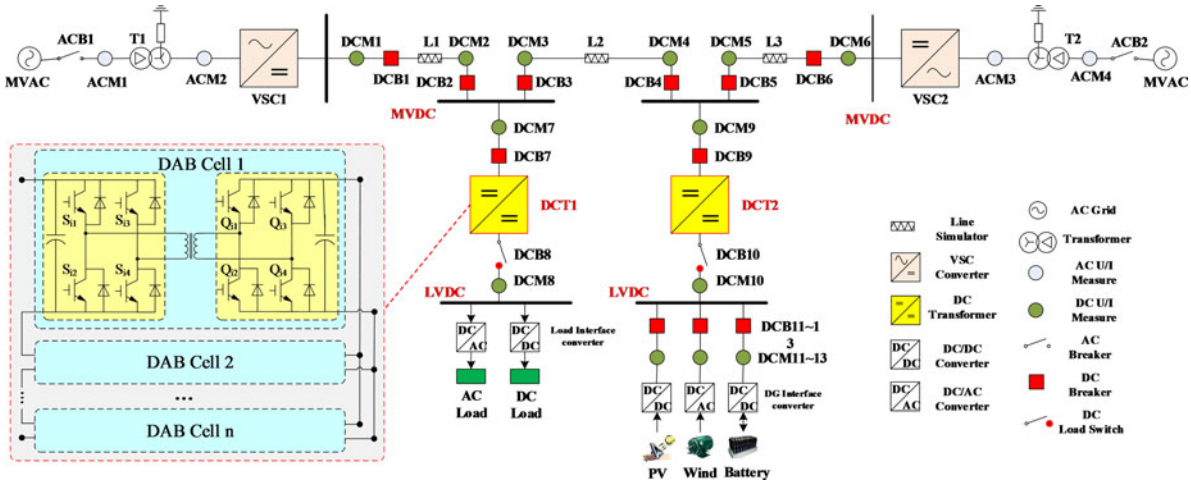

Fig. 1. Demonstration scheme for flexible MVDC distribution system.

as ease of realizing soft switching, capability for bidirectional power transfer, high power density, and modular and symmetric structure, DAB is the most suitable converter cell and can be used as base cell for DCT. On this basis, an introduction about the small-signal model of the multiple DAB was presented [25], but further studies (such as operation principle, control, design, and experiments) of multiple DABs used in DCT were not concerned.

For flexible ac power distribution, solid-state transformer (SST) is a good solution to connect MV and LV ac grid by using power electronic technology [26]–[29]. However, because the dc power distribution concept has only been focused for a short period of time, the world-wide research regarding SSTs is mainly focused on the ac SST. Although DAB-based dc–dc conversion also exists in ac SST, even the DAB-based ac SST prototype with several kilovolts was reported in literatures, but the operation, control, and fault performance are very different with DCT in flexible MVDC distribution. Moreover, although some literatures have discussed the DCT based on DAB in MVDC distribution, all of them focused only on one aspect, and the content is insufficient. In particular, issues on full-process operation, control and fault management, and experiments when DCT is applied in flexible MVDC distribution are never investigated.

In view of the situation mentioned earlier, this paper will provide a practical tutorial on the full-process operation, control, and experiments of DCT based on DAB in flexible MVDC distribution system. The paper is organized as follows. Section II provides discussion on the operation requirements for flexible MVDC power distribution and gives operation mode design of DCT. Section III presents three optimal modulations during startup, steady, and transient processes. Section IV analyzes the stability of balance control and presents a full-process control strategy during operation process. Section V discusses voltage balance issue of DCT during block process and provides an optimal solution in practice. Section VI gives a fault-handling solution for DCT. Section VII gives a practical parameter and hardware design method. Section VIII and IX present comprehensive simulations and experiments of DCT in MVDC distribution system.

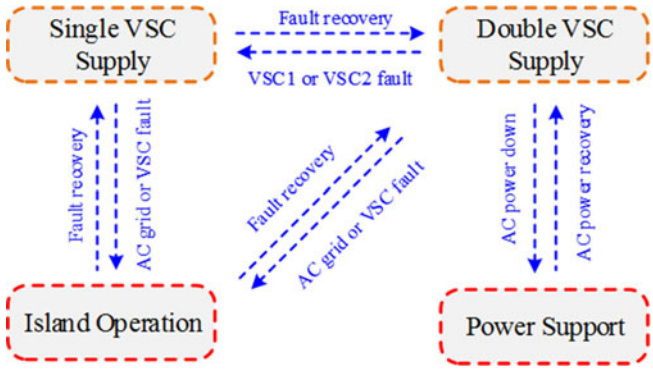

Fig. 2. Possible operation ways of MVDC distribution system.

II. Full-Process Optimal Operation of DCT for Flexible MVDC Distribution Application

A. Flexible Operation of MVDC Distribution System

In traditional ac distribution, an ac magnetic transformer just needs to achieve voltage conversion, which is determined by turn ratio, and power flow is passively determined by the load. By contrast, in flexible MVDC distribution system, different kinds of power electronic converters and distributed sources exist, as shown in Fig. 1, and the system structure can be changed into different forms according to different operational requirements.

Fig. 2 shows several possible operation ways of MVDC distribution system. When all of the components are normal, the system will operate in double VSC supply way. When a VSC breaks down and another VSC works normally, the system will operate in single VSC supply way. For both single and double VSC supply ways, the VSCs are the main converters to control the MVDC distribution grid, whereas the DCTs are the main converters to control LVDC microgrid. In addition, when only one ac grid breaks down, the system can work in power support way, where the DCTs still control the LVDC microgrid. When two ac grids or two VSCs break down, the system will shift to the island operation, where the DCTs are the main converters

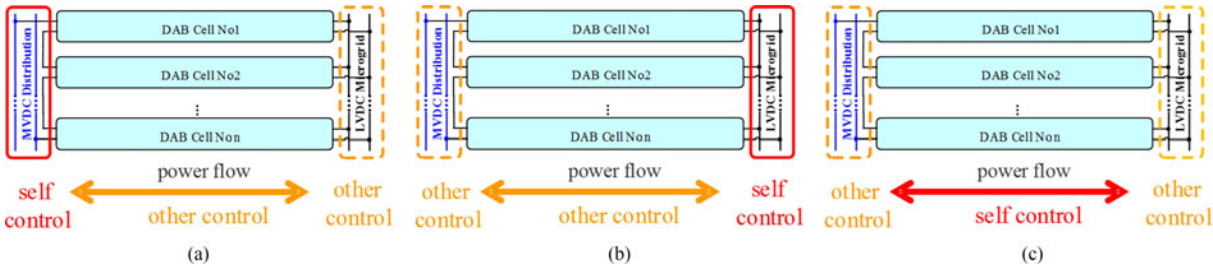

Fig. 3. Full-process operation mode design. (a) MVDC control mode. (b) LVDC control mode. (c) Power control mode.

to control MVDC distribution grid, whereas the VSCs are the main converters to control MVAC distribution grid.

There are also other operation ways which are not depicted in Fig. 2. However, no matter how to define the operation ways in flexible MVDC distribution system, the voltage and power of DCT in the flexible MVDC distribution system should be controlled actively to access various buses or distributed sources with different voltage levels.

B. Full-Process Operation Mode of DCT

According to the flexible operation requirements in MVDC distribution system, the full-process operation of DCT is designed to three modes: MVDC control, LVDC control, and power control modes, as shown in Fig. 3.

1) Mode I: MVDC Control Mode: In the MVDC control mode, the LVDC bus is controlled by the LVDC microgrid or by the dc voltage source. The MVDC bus is controlled by DCT. The amplitude and direction of the whole power of DCT is passively determined by the system in the MVDC side.

2) Mode II: LVDC Control Mode: In the LVDC control mode, the MVDC bus is controlled by the MVDC distribution grid, whereas the LVDC bus is controlled by DCT. Moreover, DCT must control the voltage sharing of each DAB cell in the series side, as well as the power sharing in the parallel side; the amplitude and direction of the whole power of DCT are passively determined by the load in the LVDC side.

3) Mode III: Power Control Mode: In the power control mode, both the MVDC and LVDC buses are controlled by dc distribution grid and dc microgrid, and the amplitude and direction of the whole power are actively controlled by DCT. Moreover, DCT must control the voltage sharing of each DAB cell in the series side and the power sharing in the parallel side.

It needs to be pointed out that the power flow of DCT in all of the aforementioned modes can be operated in either forward or reverse directions. Based on the earlier design, DCT not only achieves voltage conversion and electric isolation between different dc buses but also actively controls voltage, current, and power in MVDC distribution system.

C. Dual-Active Phase-Shift Operation Principle of DCT

The DCT in Fig. 1 is composed of multiple identical DABs connected in parallel to the LVDC bus and in series to the MVDC bus. The cell number of the DCT differed between dc buses with different voltage and power levels. In DCT, using a high-frequency (HF) transformer instead of a traditional line-frequency (LF) transformer allowed the DCT to achieve small volume, lightweight, low cost, and little noise. The modularity is also increased.

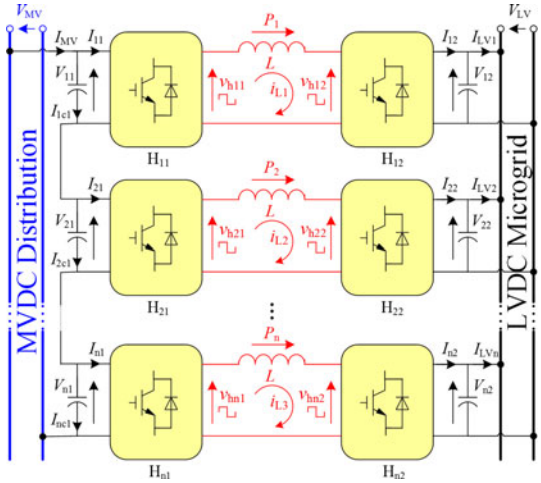

Fig. 4. Dual-active phase-shift principle of DCT.

In DCT, all DABs operate under the same principle, as shown in Fig. 4. Similar to the operation principle of power transmission in traditional ac systems, the direction and magnitude of inductor current i_{Li} can be changed by adjusting the phase shift between ac output square wave voltages v_{hi1} and v_{hi2} of full bridges, which can control the direction of power flow and magnitude of DAB in DCT. The difference is that the voltages on both sides of the inductor in traditional ac power system are LF sinusoidal waves whereas HF square waves in DAB.

It needs to point out that the power flow in DCT is bidirectional, and the concept of input and output sides, which are used in traditional multiple dc–dc converter as presented in previous literatures, are not used in this paper; rather, we define them as MVDC and LVDC sides, respectively.

In Fig. 4, L is the sum of transformer leakage inductance and the auxiliary inductor; V_{MV} and V_{LV} are MVDC and LVDC bus voltages, respectively; I_{MVi} and I_{LVi} are average currents on MVDC and LVDC sides, respectively; $V_{\mathrm{i1}}/V_{\mathrm{i2}}$ and $I_{\mathrm{i1}}/I_{\mathrm{i2}}$ are the average voltages and currents on MVDC and LVDC sides, respectively; P_i is the transmission power of each DAB cell; v_{hi1} and v_{hi2} are ac output voltages of H-bridges; i_{Li} is the ac current; T_{hs} is a half switching period; and $i = 1, 2, 3, \ldots, \mathrm{n}$.

III. Full-Process Optimal Modulation

The dual-active phase-shift power transmission principle of DCT is introduced in Section II-C. However, some issues are noted when the theoretical methods are applied in practice,

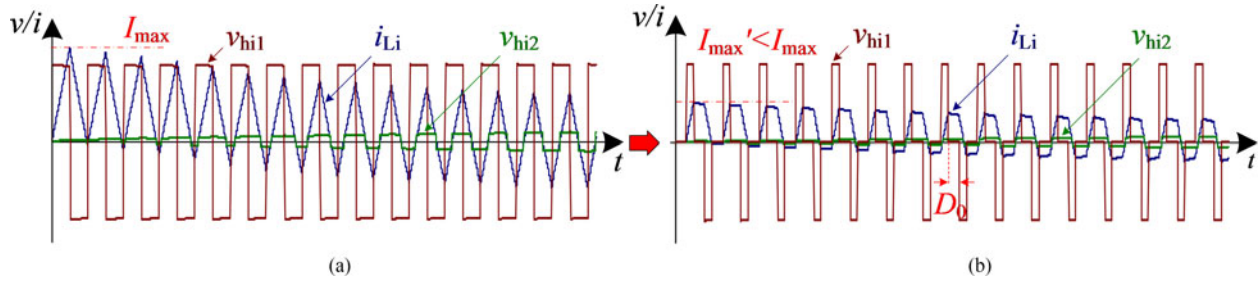

Fig. 5. Optimal modulation method for DCT during startup process. (a) Theoretical modulation. (b) Practical optimal modulation.

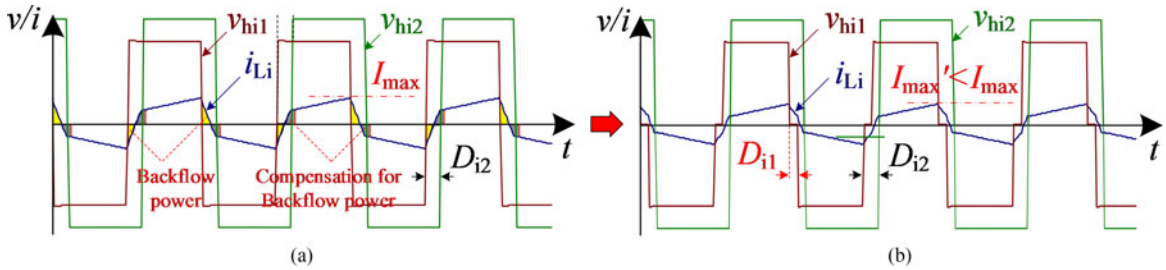

Fig. 6. Optimal modulation method for DCT during steady process. (a) Theoretical modulation. (b) Practical optimal modulation.

and thus these methods can be further improved. This section presents several practical optimal modulation methods to improve the performance of DCT under different processes.

A. Optimal Modulation During Startup Process

During startup process, the dc terminal voltage in the control side is not established and is very low. If we still employ the steady-state modulation strategy, a high current impact will occur, which may destroy power devices, as shown in Fig. 5(a), in which LVDC voltage control mode is used as example.

Given that the LVDC voltage is zero during the first switching period, the current impact $I_{\max}$ can be derived as

$$I_{\max} = \frac{V_{i1}}{L} T_{\rm hs}. \tag{1}$$

To reduce the current impact, a soft startup modulation is proposed in Fig. 5(b). During startup process, all of the switches of H-bridges in the LVDC side are turned off, which operate as uncontrolled rectifiers; all of the switches of H-bridges in the HVDC side are enabled, which operate as inverters; however, large inner phase-shift ratios D_0 for $\mathrm{H_{i1}}$ exist and generate square waves with small duty ratio. Then, the current impact $I'_{\max}$ can be derived as

$$I'_{\max} = \frac{V_{i1}}{L}(1 - D_0)T_{\rm hs} < I_{\max} \tag{2}$$

where $0 < D_0 < 1$ is the inner phase-shift ratio which takes half switching period as one unit.

Because the inner phase-shift ratio D_0 is usually designed to be sufficiently large, the duty ratio is considerably small, and even the dc terminal voltage in the control side is not established at the beginning, the overcurrent can be avoided. After the dc terminal voltage in control side is established, the soft startup process is terminated, the switches in the LVDC side are enabled, and the system shifts to steady-state process.

To speed up the startup process, we can gradually increase the inner phase-shift ratios as the increase of the dc terminal voltage. However, the increasing speed should be adjusted to ensure that the charging current is lower than the current threshold of power devices. In addition, during startup process, the closed-loop control should be disabled, and the outer phase-shift ratio should be zero to reduce the impact current when the system shifts from startup to steady-state process.

In the MVDC voltage control mode, we only need to interchange the switching states of $\mathrm{H_{i1}}$ and $\mathrm{H_{i2}}$. In the power voltage control mode, because both the MVDC and LVDC sides are provided by external sources, the steady-state modulation strategy, which does not demonstrate current impact, can be used during the startup process.

B. Optimal Modulation during Steady Process

According to the analysis presented in Section II-C, during steady process, each H-bridge generates HF square wave voltages $v_{\rm hi1}$ and $v_{\rm hi2}$ for both sides of the transformer, then the magnitude and direction of power flow of each DAB can be controlled by adjusting the outer phase-shift ratio $D_{\rm i2}$ between $v_{\rm hi1}$ and $v_{\rm hi2}$. Usually, the single-phase-shift modulation is widely used in DAB, but the backflow power is high when the dc terminal voltages don't match the transformer turn ratio, as shown in Fig. 6(a).

Assuming that $V_{\rm i1} \geq n_{\rm T} V_{\rm LV}$, the current peak $I_{\max}$ can be derived as

$$I_{\max} = \frac{n_T V_{\rm LV}[k + (2D_{i2} - 1)]}{4 f_s L} \tag{3}$$

where n_T is the transformer ratio, $k = V_{\rm i1}/n_{\rm T} V_{\rm LV}$ is the voltage conversion ratio, and f_s is the switching frequency.

Many optimal modulations have been proposed in literatures. However, all of them can be unified, and the fundamental optimal strategy can be used to determine the inner phase-shift

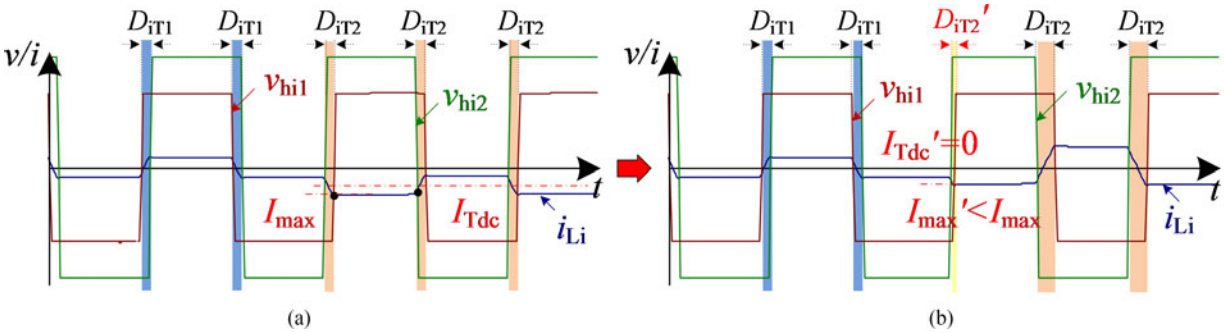

Fig. 7. Optimal modulation method for DCT during transient process. (a) Theoretical modulation. (b) Practical optimal modulation.

ratios [15], as shown in Fig. 6(b). Aside from the outer phase-shift ratio D_{i2} between the two H-bridges, another degree of freedom exists, namely, the inner phase-shift ratio D_{i1} between the diagonal switches of H-bridge. Then, the current peak $I'_{\max}$ can be derived as

$$I'_{\max} = \frac{n_T V_{\rm LV}[k(1-D_{i1})+(2D_{i2}-1)]}{4f_s L}. \tag{4}$$

The fundamental reactive power can be derived as [15]

$$Q_1 = \frac{4V_{i1}\cos(\alpha_1/2)}{\pi^3 f_s L}\left[V_{i1}\cos\left(\frac{\pi D_{i1}}{2}\right) - n_T V_{\rm LV}\cos(\pi D_{i2})\right]. \tag{5}$$

In order to ensure the outer phase-shift ratio D_{i2} operating in optimal range under the rated conditions, D_{i2} is usually designed with a small value. Thus, to eliminated the fundamental reactive power, the inner duty ratio can be designed approximately as

$$D_{i1} = \frac{2\arccos(n_T V_{\rm LV}/V_{i1})}{\pi}. \tag{6}$$

In practice, the amplitude and direction of the transmission power of DCT can be controlled by adjusting the outer phase-shift ratio, and the circulating power can be reduced by adjusting the inner phase-shift ratio. In fact, because the parameters will be changed greatly in practice, the real-time optimal modulation with close-loop is not that effective, usually the enumeration method can be used.

C. Optimal Modulation During Transient Process

In flexible MVDC application, the DCT may work in different operation modes, and the power flow is bidirectional. From [20], if the steady phase-shift modulation is still used during transient process, there will be a big transient impact $I_{\max}$ and dc bias $I_{\rm Tdc}$ in the HF-link (HFL) current, resulting in great current impact on the switches and endangers the safe operation of the converter. Fig. 7 shows the waveforms when the power flow changes from forward to reverse direction.

The current impact $I_{\max}$ can be derived as from [20]

$$I_{\max} = \frac{n_T V_{\rm LV}}{4f_s L}[2\,|D_{iT2}|\,(k+1) - 1 + k + 2D_{iT1}]. \tag{7}$$

The dc bias $I_{\rm Tdc}$ can be derived

$$I_{Tdc} = -\frac{n_T V_{\rm LV}}{4f_s L}\left[2(k\,|D_{iT2}| + D_{iT1})\right]. \tag{8}$$

To eliminate the dc bias and current impact during transient process, the optimal transient modulation can be used [20], as shown in Fig. 7(b). When there is a big step for outer phase-shift ratio between two adjacent switching periods, we can adjust the phase change of $v_{\rm hi2}$ into two parts ($\rm D'_{iT2}$, $\rm D_{iT2}$) in subsequent switching period; the two parts are then added to the rising and falling edges of $v_{\rm hi2}$, respectively. Then, the dc bias $I'_{\rm Tdc}$ can be derived

$$I'_{\rm Tdc} = \frac{n_T V_{\rm LV}}{4f_s L}(2D_{iT1} + 4D'_{iT2} - 2\,|D_{iT2}|)k. \tag{9}$$

In order to eliminate the dc bias, we set $I_{\rm Tdc}=0$, we have

$$D_{iT2}{}' = \frac{|D_{iT2}| - D_{iT1}}{2}. \tag{10}$$

Then

$$I'_{\max} = \frac{n_T V_{\rm LV}}{4f_s L}[(1+k)\,|D_{iT2}| - 1 + k] < I_{\max}. \tag{11}$$

In fact, to adjust the phase change of $v_{\rm hi2}$ to two parts ($\rm D'_{iT2}$, $\rm D_{iT2}$) in the subsequent switching period, the voltages of the transformer become symmetry over one switching period, so the current impact and dc bias are eliminated.

IV. Full-Process Optimal Control of DCT During Operation Process

As presented in Section III, there are three operation modes for DCT in flexible MVDC application. In all the modes, DCT must control the voltage balance of each series DAB cell, as well as the power balance of each parallel DAB cell.

A. Voltage and Power Balance Principle

From Fig. 3, the currents in the series side are equivalent and the voltages in parallel side are equivalent, it can be derived as

$$\begin{cases} V_{\rm MV} = V_{11} + V_{21} + \cdots + V_{n1} \\ I_{\rm MV} = I_{\rm MV1} = I_{\rm MV2} = \cdots = I_{{\rm MV}n} \\ V_{\rm LV} = V_{12} = V_{22} = \cdots = V_{n2} \\ P_{\rm DCT} = P_1 + P_2 + \cdots + P_n \end{cases}. \tag{12}$$

Ignoring power loss, the average current across the dc capacitor over one switching period should be zero in the steady state;

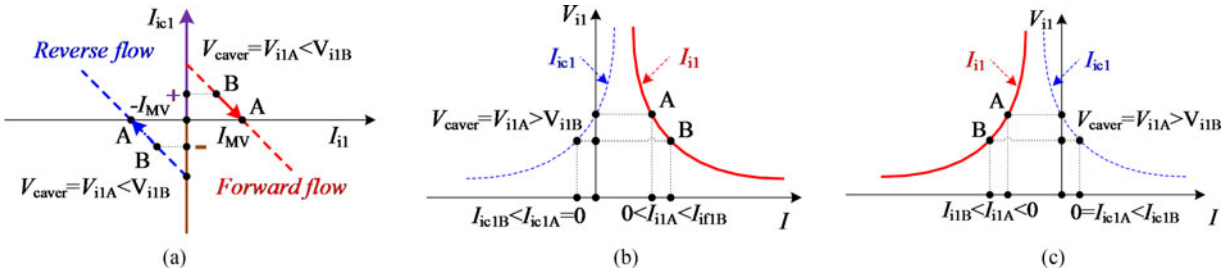

Fig. 8. Balance control stability analysis of DCT for flexible MVDC application during operation process. (a) Voltage balance control. (b) Power balance control with forward power flow. (c) Power balance control with reverse power flow.

then

$$I_{\mathrm{MV}i} = I_{i1} \quad \text{and} \quad I_{LVi} = I_{i2}. \tag{13}$$

The input and the output average power are the same, and we have

$$P_i = V_{i1} I_{i1} = V_{i2} I_{i2}. \tag{14}$$

From (12) to (14), we have

$$V_{11} = V_{21} = \cdots = V_{n1} \Leftrightarrow P_1 = P_2 = \cdots = P_n. \tag{15}$$

From (15), the voltage balance of each series DAB cell in the MVDC side and the power balance of each parallel DAB cell in the LVDC side are also theoretically equivalent, and this conclusion still holds in both the forward and reverse power flows in all of the modes. This finding indicates that we only need to control one of the voltage balance in the MVDC side and the power balance in the LVDC side.

B. Balance Control Stability

According to the earlier analysis, the voltage balance of each series DAB cell in the MVDC side and the power balance of each parallel DAB cell in the LVDC side are theoretically equivalent. However, the two methods have different control stabilities in practical control.

In fact, assuming that the inner phase-shift ratio $D_{\mathrm{i}1} = 0$, for each DAB cell in DCT, the transmission power can be derived as

$$P_i = \frac{n_T V_{\mathrm{i}1} V_{\mathrm{LV}}}{2 f_s L} [D_{i2}(1 - D_{i2})]. \tag{16}$$

From (16), the series voltage and power of each DAB cell can be adjusted by the outer phase-shift ratio. Taking positive power flow to analyze, if the voltage balance control is used, when the power of DAB cell is high, the outer phase-shift ratio will be increased to ensure voltage balance; if the power balance control is used, when the series voltage of DAB cell is high, the outer phase-shift ratio will be decreased to ensure power balance.

1) Voltage Balance Control: Assuming that the system voltage and load current are constant, when the control for the series voltage balance is used, the dynamic process is shown in Fig. 8(a).

When the power is in the forward flow, the DABi in the initial state operates stably in point A; thus, $V_{\mathrm{i}1} = V_{\mathrm{caver}}$, $I_{\mathrm{ic}1} = 0$, and $I_{\mathrm{i}1} = I_{\mathrm{MV}}$, where V_{caver} is the average voltage of the series capacitors and $I_{\mathrm{ic}1}$ is the current flowing to the series capacitor. Assuming that the disturbance reduces the power, due to the parallel connection in LVDC side, the current $I_{\mathrm{i}2}$ will decrease, then $I_{\mathrm{i}1}$ will decrease. Because the series current I_{MV} is constant, the operation point is changed from *A* to *B*. The capacitor current $I_{\mathrm{ic}1}$ is changed from zero to above zero, and then the capacitor is charged and the voltage is higher than V_{caver}. Then the series voltage balance control will be enabled, the outer phase-shift ratio will be increased, and the capacitor current $I_{\mathrm{ic}1}$ will be reduced to balance the capacitor voltage; then the feedback is produced, the current $I_{\mathrm{i}1}$ and $I_{\mathrm{i}2}$ will increase, and the power will recover to the balance.

When the power is in the reverse flow, the DABi in the initial state operates stably in point A; thus $V_{\mathrm{i}1} = V_{\mathrm{caver}}$, $I_{\mathrm{ic}1} = 0$, and $I_{\mathrm{i}1} = -I_{\mathrm{MV}}$. Assuming that the disturbance reduces the power, due to the parallel connection in LVDC side, the current $|I_{\mathrm{i}2}|$ will decrease, then $|I_{\mathrm{i}1}|$ will decrease. Because the series current I_{MV} is constant, then the operation point is changed from *A* to *B*. The capacitor current $I_{\mathrm{ic}1}$ is changed from zero to below zero, then the capacitor is discharged and the voltage is lower than V_{caver}. Then the series voltage balance control will be enabled, the outer phase-shift ratio will be increased with negative polarity, and the capacitor current $|I_{\mathrm{ic}1}|$ will be reduced to balance the capacitor voltage, then the feedback is produced, the current $|I_{\mathrm{i}1}|$ and $|I_{\mathrm{i}2}|$ will increase, and the power will recover to the balance.

2) Power Balance Control: When the control for power balance is employed, the dynamic process with forward flow is shown in Fig. 8(b). In the initial state, the DABi operates stably in point A, thus $V_{\mathrm{i}1} = V_{\mathrm{caver}}$, $I_{\mathrm{i}1} = I_{\mathrm{MV}}$, and $I_{\mathrm{ic}1} = 0$. Assuming that the disturbance cause the decrease of the capacitor voltage $V_{\mathrm{i}1}$, then $I_{\mathrm{i}1}$ increases, and the operation point is changed from *A* to *B*; because the series current I_{MV} is a constant, the capacitor current $I_{\mathrm{ic}1}$ is changed from zero to below zero, then the capacitor is discharged and the voltage is further decreased. Therefore, positive feedback is produced, the capacitor voltage continues to decrease until it becomes zero, and then the power balance is disrupted.

When the power is in the reverse flow, the dynamic process is shown in Fig. 8(c). Assuming that the disturbance cause the decrease of the capacitor voltage $V_{\mathrm{i}1}$, then $|I_{\mathrm{i}1}|$ increases, the operation point is changed from *A* to *B*; because the series current I_{MV} is a constant, the capacitor current $I_{\mathrm{ic}1}$ is changed from zero to above zero, then the capacitor is charged and the voltage is increased. Therefore, negative feedback is produced, the capacitor voltage recovers to the balance.

According to the earlier analysis, the power balance can be always achieved when the voltage balance control in the series

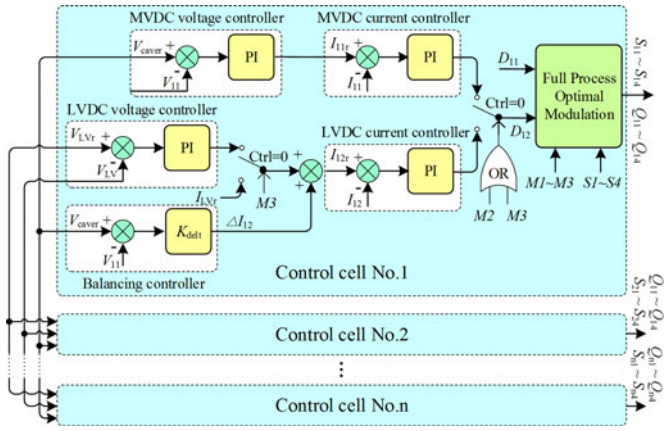

Fig. 9. Full-process control strategy of DCT for flexible MVDC application during operation process.

side is used; the voltage balance in the series side can be achieved in the reverse power flow when the power balance control is used, however the DCT will be unstable in the forward power flow.

C. Full-Process Control Design During Operation Process

In order to enhance the stability and dynamic performance, a full-process control strategy of DCT in flexible MVDC application during operation process is proposed in Fig. 9. $M1-M3$ are binary logic control signals for the MVDC control mode, the LVDC control mode, and the power control mode, respectively; when these parameters are equal to 1, the corresponding mode is enabled. In the control strategy, each DAB cell has an identical control model and non-master-slave relationship; each control cell consists of an MVDC voltage controller, an MVDC current controller, an LVDC voltage controller, an LVDC current controller, and a balancing controller.

In the MVDC control mode, the LVDC bus voltage is constant, the MVDC voltage reference V_{MVr} is given, the MVDC voltage and current controllers are enabled, and the average voltage V_{caver} is calculated as (17). The MVDC voltage controller takes the difference between V_{i1} and V_{caver} as the input to the PI controller, and the output is used as current reference I_{1ir} for the MVDC current controller. The MVDC current controller takes the difference between I_{i1} and I_{i1r} as input for the PI controller, and the output is used as the outer-phase-shift ratio. In the MVDC control mode, the series MVDC voltage is controlled by each DAB cell. Thus, the balancing controller is not needed, and the voltage balance in MVDC side can be achieved easily. According to the analysis in the last section, the power balance in the LVDC side can also be achieved. In the MVDC control mode, the amplitude and direction of the power are passively determined by the system in the MVDC side

$$V_{\mathrm{caver}}=\begin{cases}V_{\mathrm{MVr}}/n & M1=1\\ (V_{11}+V_{21}+\cdots+V_{\mathrm{n1}})/n & M2=1 \ \text{ or } \ M3=1\end{cases}. \tag{17}$$

In the LVDC control mode, the LVDC voltage controller takes the difference between V_{LV} and the reference value V_{LVr} as input for the PI controller, and the output is used as the unified current reference for the LVDC current controller for each DAB cell. The MVDC balancing controller collects the dc voltages V_{i1} in the series side, and calculates the average voltage V_{caver}. It needs to be pointed out that V_{caver} in the MVDC control mode is calculated according to real-time detection; in the LVDC control mode, V_{caver} is calculated according to the given reference.

On this basis, the MVDC balancing controller further calculates the correcting value $\triangle I_{\mathrm{i2}}$ for the unified current reference. The sum of the unified current reference and $\triangle I_{\mathrm{i2}}$ is the current reference for each DAB cell.

In the MVDC balancing controller, the calculation of $\triangle I_{\mathrm{i2}}$ does not contain an integral function, it can be derived as

$$\begin{cases}\Delta I_{\mathrm{i2}}=K_{\mathrm{delt}}(V_{\mathrm{caver}}-V_{i1})\\ \Delta I_{12}+\Delta I_{22}+\cdots+\Delta I_{n2}=0\end{cases} \tag{18}$$

where K_{delt} is the proportional control parameter.

It can be seen from (18), the sum of the correcting values of all the DAB cells is equal to zero. Thus, the MVDC balancing controller exerts no effect on the control of the LVDC bus voltage. The trial and error method can be used for K_{delt} to gain satisfactory steady and transient operating performances in actual engineering projects.

In the power control mode, the control status of the DCT is similar to that of the LVDC control mode; the only differences are that the MVDC and LVDC bus voltages are constant, only the LVDC current controller and balancing controller are enabled, and the unified current reference I_{LVr} is directly calculated from the given power reference.

According to the earlier analysis, to obtain a different power flow direction, we only need to change the polarity of the phase-shift ratio but not the states of the switches. Thus, the same control scheme can be used in both the forward and reverse directions of all the modes.

V. Full-Process Optimal Control of DCT During Block Process

Section IV gives an analysis on balance control during operation process. In addition to normal operation process, there is also block process (includes standby, startup and fault states in Section VII), which also exists for a long time in flexible MVDC application [30].

A. Voltage Balance Issue During Block Process

During block process, the driving signals of power switches are locked, no output power is generated by the DCT. However, the control system should be powered normally to provide human–computer interaction and have the ability to restore operation quickly at any time.

Different with ac distribution grid, dc distribution grid lacks ac link, the control power source (CPS) of each DAB just obtains power from dc capacitor. In practice, the CPSs for two H-bridges of primary and secondary sides of the transformer are isolated, the CPSs in primary side are connected to the capacitors in MVDC side whereas the CPSs in the secondary side are connected to the capacitors in LVDC side, so it can meet the high voltage isolation specification.

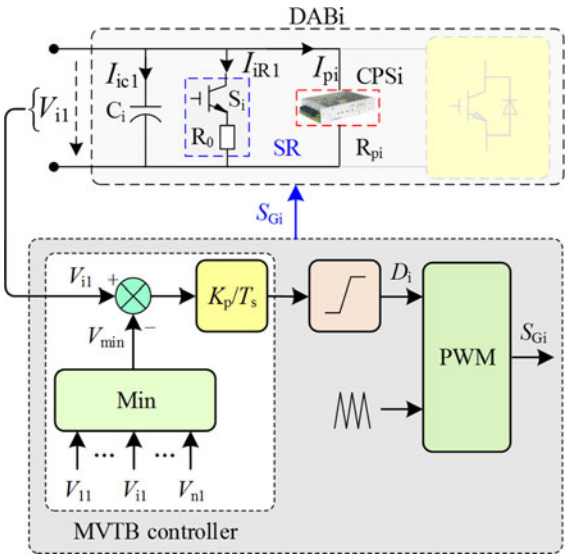

Fig. 10. Full-process control strategy of DCT for flexible MVDC application during block process.

In MVDC control mode, the voltage in MVDC side is not established at first; the CPS in LVDC side will operate first to drive the H-bridges that operate as inverters, and then the H-bridges in MVDC side operate as rectifiers, causing the dc capacitors in MVDC side to be charged. After a certain amount of time, when the voltages of dc capacitors achieve the operating voltage of the CPSs, the CPSs in MVDC side will start to work, and DCT can shift into normal operation. In LVDC control mode, the voltage in LVDC side is not established at first, the operation sequence of CPSs and H-bridges in primary and secondary will interchange. For power control mode, the CPS can get power from dc capacitors both in MVDC and LVDC sides, both CPSs can operate at first.

Because the capacitors in LVDC side are connected in parallel, so there is no voltage and power balance issue in MVDC and power control modes. However, in LVDC control mode, the CPSs in MVDC side get power from each series capacitor; due to inverse effect between voltage and current of CPSs, the voltage balance will be destroyed when slight difference exists between different CPSs.

B. Optimal Balance Control Solution for DCT During Block Process

In the tradition solution, a balance resistor is added in parallel with each dc capacitor. To ensure the direct relationship of resistor can offset the inverse relationship of CPS, the dissipation power of auxiliary resistor should equal to the dissipation power of CPS.

In fact, we don't need to use the direct effect of resistor to completely offset the inverse effect of CPS. We only need to ensure that the power generated by each series capacitor is the same, and then the series voltage can be balanced. From [30], in order to reduce power loss of traditional solution, a minimum voltage tracking balance (MVTB) control can be used, as shown in Fig. 10. A switch S_i with small current level is added to the resistor. Thus, the power loss of the resistor can be adjusted by S_i.

In MVTB control, each cell will compare its own series voltage V_{i1} with the minimum voltage $V_{\min}$, where $V_{\min} = \min V_{11}, V_{21}, \ldots, V_{n1}$. The switch S_i will be turned on and the resistor expend energy from the series side when $V_i > V_{\min}$. Moreover, the larger the difference between V_i and $V_{\min}$, the longer the on time of S_i and the larger the dissipated energy of the resistor. Because the closed loop is employed, voltage imbalance can be eliminated and power loss can be reduced.

Assuming that the initial series voltages are the same. When the CPSs startup, the series voltage with small dissipated power will increase, the current will decrease resulting from the constant power characteristic of CPS, and then the series voltage will further increase. At this time, the resistor is switched into operation, the resistor absorbs power from the series voltage, and thus, the voltage decreases.

In order to ensure voltage balance, in steady state, we have

$$P_{Ri} = P_{p\max} - P_{\mathrm{pi}} \quad \text{and} \quad P_{Ri} = \int_0^{T_s} V_i I_{Ri} \mathrm{d}t = D_i \frac{V_i^2}{R_0^2}. \quad (19)$$

From (19), the power loss of resistor is simply the power difference between different CPSs, and the resistance should be designed to consume the maximum power difference. The smaller the resistance, the faster the recovery speed, but the current impact of S_i will be high and the power loss is constant.

According to the earlier analysis, because there are many operation modes for DCT in flexible MVDC distribution, we must ensure that the CPSs can get power from both MVDC and LVDC sides in practice. In addition, the tracking balance control can reduce power losses greatly compared with the traditional solution.

VI. Fault-Handing Solution of DCT for Flexible MVDC Distribution Application

A. Fault Issue of DCT for MVDC Distribution

In MVDC distribution application, the MVDC voltage is about tens of kV, the cell number will be dozens, which increases the failure rate of the DCT. In order to enhance the reliability of the system, the DCT should have the fault-handing ability.

For the DCT in Fig. 1, due to the existence of concentrated capacitor, the DCT cannot operate with redundant unit when a cell fails, otherwise the dc capacitor of the faulted cell will be short-circuited, which reduces the system reliability, especially in MVDC application. In addition, the DCT cannot disconnect fully from MVDC distribution when a short fault occurs in the distribution bus, the dc capacitor will be discharged rapidly and a large overcurrent will occur. When the fault is eliminated, the dc capacitor must be recharged and the fault recovery is slow.

B. Fault-Handing Solution of DCT for MVDC Distribution

Fig. 11 shows a fault-handing solution of DCT for flexible MVDC distribution application. Every capacitor is connected to a switch, in which a bypass contactor is connected in parallel to H-bridge in MVDC side. Due to the parallel connection in LVDC side, so the bypass contactor is not needed. Based on

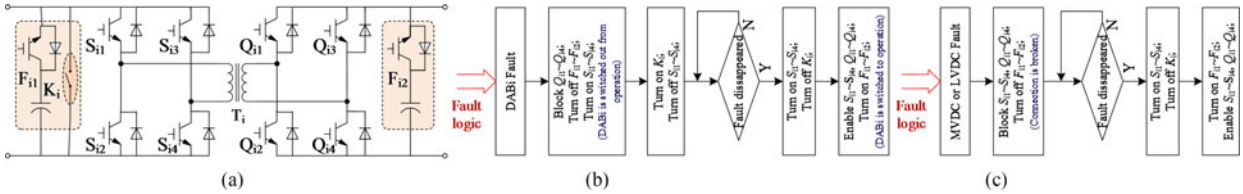

Fig. 11. Fault-handing solutions of DCT for flexible MVDC distribution application. (a) Practical structure. (b). Fault logic with internal fault. (c) Fault logic with external fault.

this, the concentrated capacitor of DCT is changed to switched capacitor.

In normal operation, the switches $F_{11} - F_{n1}$ are turned on, whereas all bypass contactors $K_1 - K_n$ are turned off. When a failure occurs in DABi, the switches $Q_{i1}-Q_{i4}$, F_{i1} and F_{i2} are turned off immediately, the switches $S_{i1}-S_{i4}$ of H_{i1} are turned on, then the DABi is switched off and the dc capacitors will not discharge. After that, the bypass contactor K_i is turned on and the switches $S_{i1}-S_{i4}$ are turned off to reduce power loss. However, to absorb voltage peak, there will be snubber capacitor which connected to the dc-link or CE of switches. Usually, if the snubber capacitance is very small, the effect of the snubber capacitance on fault-handling method usually can be ignored considering the turn on delay time of switches. Of course, if the capacitance is several μF, before the shoot-through of the switches, the switches can be turned on and off alternately, the snubber capacitor will be discharged quickly because of the power loss of the switches and parasitic resistance in the circuit.

When a short fault occurs in the MVDC or LVDC buses, all the switches $S_{i1}-S_{i4}$, $Q_{i1}-Q_{i4}$, and $F_{i1} - F_{i2}$ are turned off, then the DCT can break the connection between MVDC and LVDC buses without the help of dc breaker, and no surge current appears. Beside these, the voltages of dc capacitors are all maintained, so after the transient short fault disappears, the DCT can restore very quickly.

According to the earlier analysis, the proposed solution not only can switch out the faulted cell quickly while the system still runs normally, but also can disconnect electrical connection between MVDC and LVDC buses quickly when some external faults occur, which improves the reliability of the system.

VII. Practical Parameter and Hardware Design of DCT for Flexible MVDC Distribution Application

A. Parameter Design

In DCT, in order to ensure the control effect, the parameters of each DAB cell are designed to be consistent. The rated voltage V_{MV} and V_{LV} of MVDC distribution grid and LVDC microgrid are determined directly according to the actual demand. The rated voltage of DAB cell in the series side is equal to V_{MV}/n and that in the parallel side is equal to V_{LV}. The number n of series cell is determined by the V_{MV} and designed voltage V_{IGBT} of switches, which is n V_{MV}/V_{IGBT}. In order to reduce the circulating current and to increase the efficiency, the transformer turns ratio n_T should match the voltage conversion ratio of DAB, that is, $n_T = (V_{MV}/n)/V_{LV}$.

In order to ensure reliable operation of DCT, the design of auxiliary inductance L and switching frequency f_s must satisfy

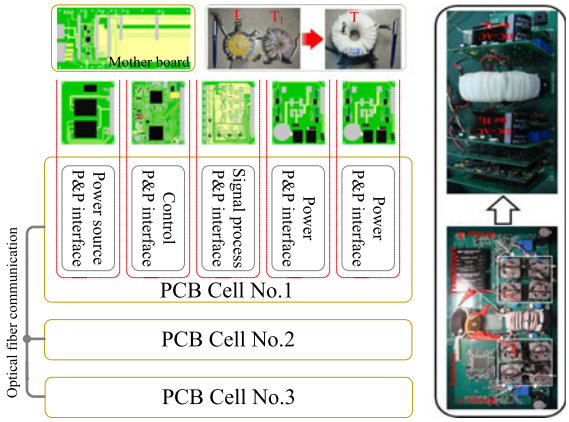

Fig. 12. Distributed and modular design strategy of DCT for flexible MVDC distribution application.

that the transmission power of DCT can achieve the rated power of load, so the minimum value of the theoretical maximum power should be larger than the rated power of load. From [19], we have

$$\frac{n_T V_{MV\_min} V_{LV\_min}}{8 f_s L} \geq \lambda P_N \tag{20}$$

where P_N is rated power of load, λ is margin coefficient, $V_{MV_{min}}$ and $V_{LV_{min}}$ are the minimum value of V_{MV} and V_{LV}, respectively, usually the maximum voltage fluctuating range is 5%−10%.

The switching frequency f_s is determined by the characteristics of the switches; the recommended operation range can be obtained from datasheet; the value is usually below 20 kHz for silicon switches.

B. Modular Hardware Design Strategy

In MVDC distribution application, the cell number will be dozens; from [19], the distributed and modular hardware design can be used to enhance the flexibility and power density. Fig. 12 shows a hardware design strategy of DCT prototype in this paper, which has a certain demonstration significance.

The flat and integrated structure of the hardware system can be improved into modular and plug and play (P&P) structure, which increases power density, modularity, and flexibility. All of the DAB cells have identical control and power systems. The control system for each cell is divided into a source module, a control module, and a signal process module. In the power system, each bridge of the DAB is designed into a power module, and the auxiliary inductor and HF transformer are integrated into a magnetic component. Then, each DAB cell is made of one source module, one control module, one signal process signal,

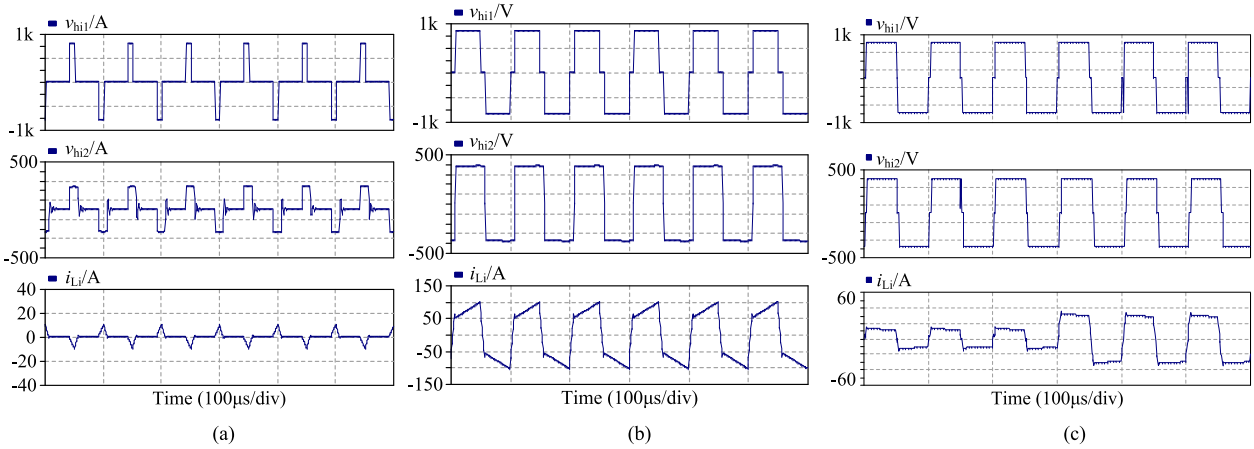

Fig. 13. Simulation results of optimal modulation for DCT during different processes. (a) Startup process. (b) Steady process. (c) Transient process.

two power modules, and one integrated HF transformer. In the PCB design, all of the modules are plugged into a mother board with a P&P interface. The signal communication between control and power systems is achieved by a mother board, and communication between the DAB cells is achieved through fiber-optic lines.

VIII. Simulation Verification of DCT for MVDC Distribution Application

To demonstrate the full-process operation of DCT for MVDC distribution application, a simulation platform of DCT with 25 DAB cells is built. The MVDC voltage $V_{\mathrm{MV}} = 20\,\mathrm{kV}$, the LVDC bus voltage $V_{\mathrm{LV}} = 380$ V, the MVDC rated voltage of DAB is $V_{\mathrm{i1}} = 20\,\mathrm{kV}/\,25 = 800\,\mathrm{V}$, the rated power for each DAB cell is 160 kW, then the rated power for the DCT is $P = 25^{*}$ 160 kW = 4 MW, the switching frequency $f_s = 10\,\mathrm{kHz}$, the transformer turns ratio $n_T = 2{:}1$, and the auxiliary inductor $L = 25\,\mu\mathrm{H}$.

Fig. 13 shows simulation waveforms of optimal modulation for DCT during different processes. It can be seen that the duty ratios of HFL voltages are far smaller than 50%, which decrease the current impact during startup process. An inner phase-shift ratio is added to the HFL voltage during steady process to decrease the circulating current. When the power is changed suddenly, the HFL current can recover to steady state within one switching period, especially there is also no current impact.

Fig. 14 shows simulation waveforms of startup and balance control for DCT. During the startup process, the DCT can operate well without current impact. All the series voltages of DCT in MVDC side keep the same, which shows a good balance effect. The LVDC voltage also keeps a constant value.

Fig. 15 shows simulation waveforms of steady operation for DCT in MVDC voltage control mode. It can be seen that the MVDC voltage is controlled with 20 kV; the voltage and power conversion for MVDC distribution and LVDC microgrid operate well. All the HFL currents of DAB cells are equivalent, which reflects a good current share effect.

Fig. 16 shows simulation waveforms of steady operation for DCT in LVDC voltage control mode. It can be seen that the LVDC voltage is controlled with 380 V; the voltage and power conversion for MVDC distribution and LVDC microgrid operate

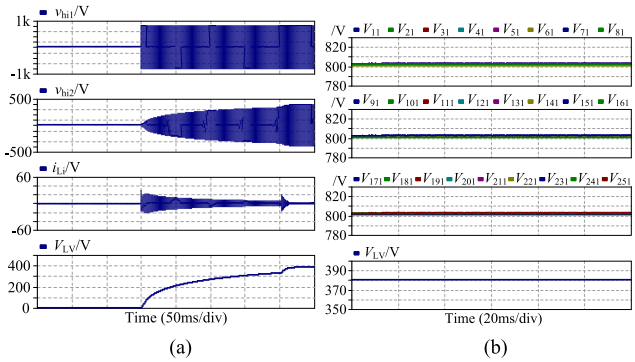

Fig. 14. Simulation results of startup and balance control for DCT. (a) Startup process. (b) Balance control.

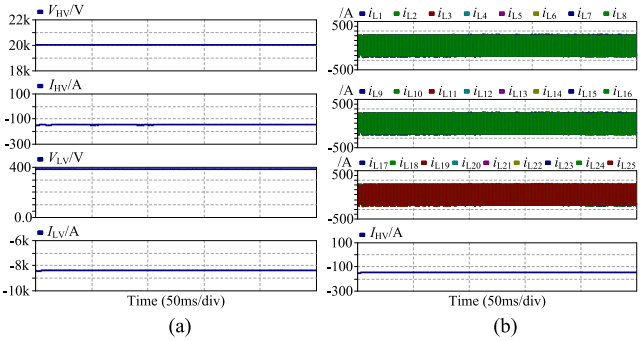

Fig. 15. Simulation results of steady operation for DCT in MVDC voltage control mode. (a) MVDC and LVDC voltage and current. (b) HFL current.

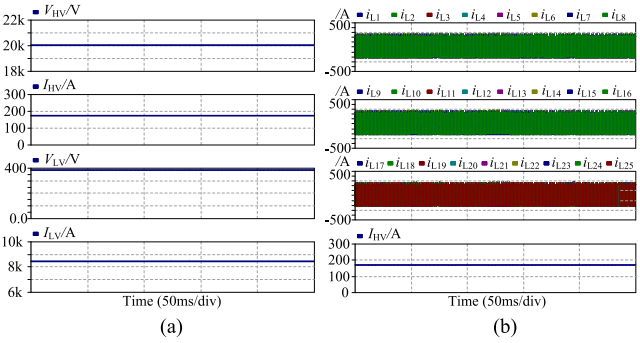

Fig. 16. Simulation results of steady operation for DCT in LVDC voltage control mode. (a) MVDC and LVDC voltage and current. (b) HFL current.

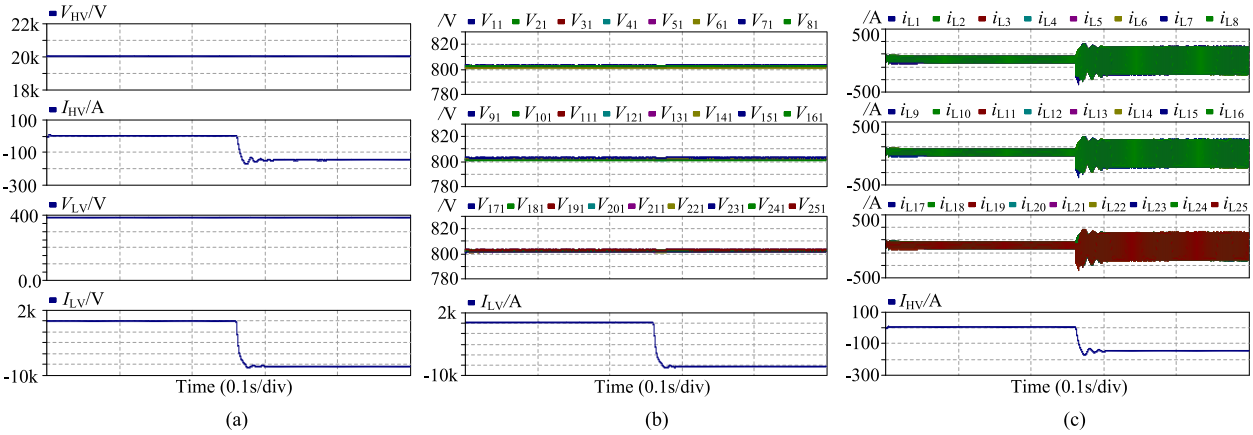

Fig. 17. Simulation results of transient operation for DCT in MVDC voltage control mode. (a) MVDC and LVDC voltage and current. (b) Series voltage. (c) HFL current.

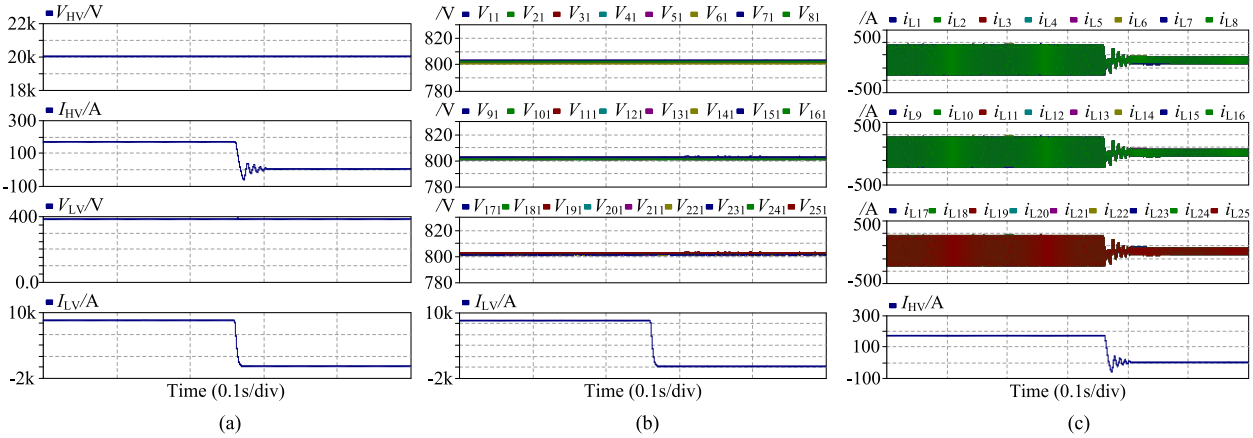

Fig. 18. Simulation results of transient operation for DCT in LVDC voltage control mode. (a) MVDC and LVDC voltage and current. (b) Series voltage. (c) HFL current.

well. All the HFL currents of DAB cells are equivalent, which reflects a good current share effect.

Fig. 17 shows simulation waveforms of transient operation for DCT in MVDC voltage control mode. It can be seen that the MVDC voltage has a good stability when the power suddenly changed, the series voltages of each DAB keep a good balance effect, and the HFL current also keeps a good share effect. The system can change to another steady operation quickly.

Fig. 18 shows simulation waveforms of transient operation for DCT in LVDC voltage control mode. The regulation is similar to the MVDC control mode; the LVDC voltage has a good stability when the power suddenly changed, the series voltages of each DAB keep a good balance effect, and the HFL current also keeps a good share effect. The system can change to another steady operation quickly.

IX. Small-Scale Prototype and Experiments

A. Prototype Implement

Fig. 19 shows an implement prototype, which is composed of three DAB cells. The rated power for each DAB cell is 1.5 kW, then the rated power for the DCT is $P = 3^{*}1.5 = 4.5\,\text{kW}$. The MVDC bus voltage $V_{\text{MV}} = 720\,\text{V}$, the LVDC bus voltage $V_{\text{LV}} = 380\,\text{V}$, the switching frequency $f_s = 20\,\text{kHz}$, the transformer turns ratio $n_T = 240{:}\,380$, and the auxiliary inductor $L = 90\,\mu\text{H}$. In experiments, the MV side of DCT is connected to the dc side of a bidirectional PWM ac–dc converter, and the ac side of this converter is directly connected to a 380-V three-phase ac grid.

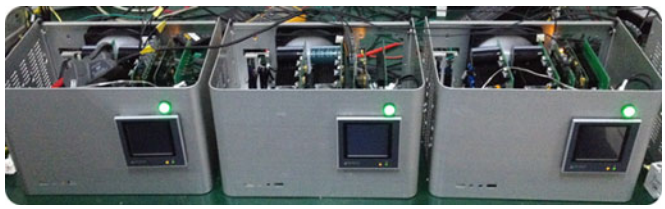

Fig. 19. Prototype photo of DCT.

The DCT employs the distributed and modular design strategy as shown in Fig. 12. Each DAB cell is designed as a separate module, and it not only can work independently but also can be composed as a DCT to work in the three modes mentioned earlier. In order to further increase the efficiency and the power density, all of the power devices are 1200 V/20 A SiC-based devices. Compared with Si-based devices, SiC-based devices

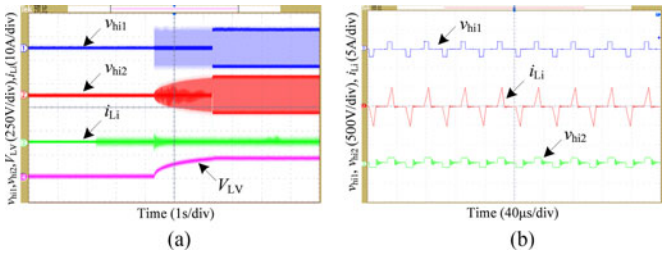

Fig. 20. Experimental results of optimal modulation for DCT during startup process. (a) Startup process. (b) Optimal modulation.

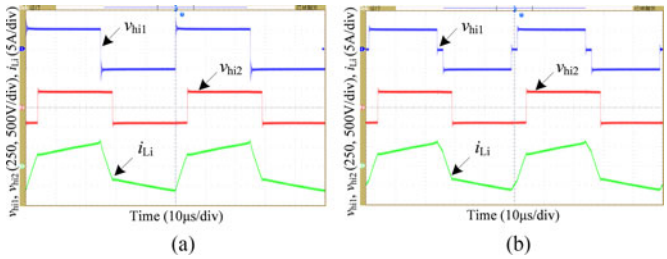

Fig. 21. Experimental results of optimal modulation for DCT during steady process. (a) Traditional modulation. (b) Optimal modulation.

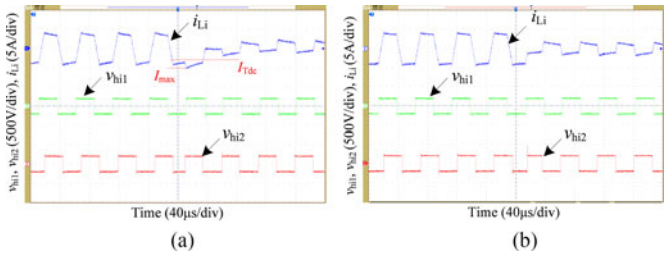

Fig. 22. Experimental results of optimal modulation for DCT during transient process. (a) Traditional modulation. (b) Optimal modulation.

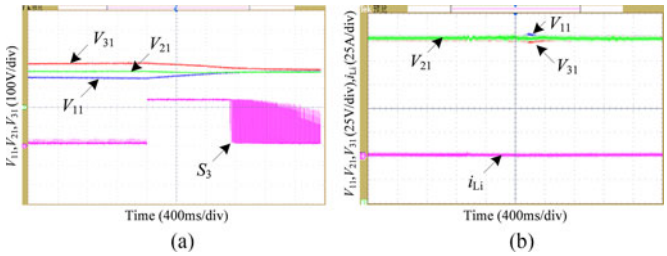

Fig. 23. Experimental results of balance control for DCT during different processes. (a) Block process. (b) Operation process.

have higher thermal conductivity, higher critical field strength, and lower carrier concentration, which are commonly considered as a key to increase efficiency and power density for HFL power conversion systems. Nowadays, the SiC-based devices from Cree and Rohm are available in the range of 1.2–1.7 kV and 100–300 A in the market.

In Section V-C, it is required to measure the dc-link current that passes the dc-link capacitor to control the DCT, which should have delicate consideration. In the hardware implement of this paper, an LEM current sensor (LA25-P) is used to measure dc-link HF current, and the current is converted into voltage signal which is suitable for the measurement of the sampling chip ADS803, which is a high-speed, high dynamic range, 12-bit/5 MHz pipelined analog-to-digital converter. This high-bandwidth, linear track/hold minimizes harmonics and has low jitter, leading to excellent signal-to-noise ratio (SNR) performance. In the controller, an FPGA (XC3S500E) and a DSP (TMS320F2812) are used, the analog to digital conversion was triggered 2 μs once, and we can get the digital result $X_{\rm i}$. At the same time, a multiplier is used to calculate its square, and we can get the digital square result $X_{\rm i}{}^2$, then the sum of 25 calculated results is calculated in FPAG and transferred to DSP, so we can calculate the square root and get the current measured result.

B. Optimal Modulation Experiments

Fig. 20 shows the experimental results of optimal modulation for DCT during startup process, which takes LVDC control as an example. During startup process, the dc terminal voltage in the control side is not established completely. All of the switches of H-bridges in the LVDC side are turned off and operate as uncontrolled rectifiers; all of the switches of H-bridges in the HVDC side are enabled and operate as inverters. Especially, there is a big inner phase-shift ratio for $H_{\rm i1}$ to generate square waves with small duty ratio, so the HFL overcurrent is avoided. After the dc terminal voltage in control side is established, the soft startup process is terminated, and the driving pulses can be enabled with normal 50% duty ratio, and the system shifts to steady-state process.

Fig. 21 shows the experimental results of optimal modulation for DCT during steady process. When the dc terminal voltages don't match the transformer turn ratio, there will be a great reactive power with traditional single-phase-shift modulation, and the current stress will be high. In optimal modulation, there is an inner phase-shift ratio in the HFL voltage, the current rising rate is reduced during this period, and the peak current is decreased.

Fig. 22 shows the experimental results of optimal modulation for DCT during transient process. During transient process, the power flow is changed from forward to reverse direction. There is a big transient impact $I_{\rm max}$ and dc bias $I_{\rm Tdc}$ in HFL current if the steady phase-shift modulation is still used during transient process, which causes a great current impact on the switches and endangers the safe operation of the converter. In optimal modulation, because the phase-shift ratio is changed into two parts during two adjacent period, the voltages of the transformer become symmetrical within one switching period, and the current impact and dc bias are eliminated.

C. Balance Control Experiments

Fig. 23 shows the experimental results of balance control for DCT during different processes. During block process, the series voltages are unbalanced resulting from parameter differences, then the MVBC is enabled, the switch $\rm S_3$ is turned on to absorb the power difference, the series voltages are then balanced, and the duty ratio of $\rm S_3$ decreases gradually. During block process, all the driving pulses and the steady balance

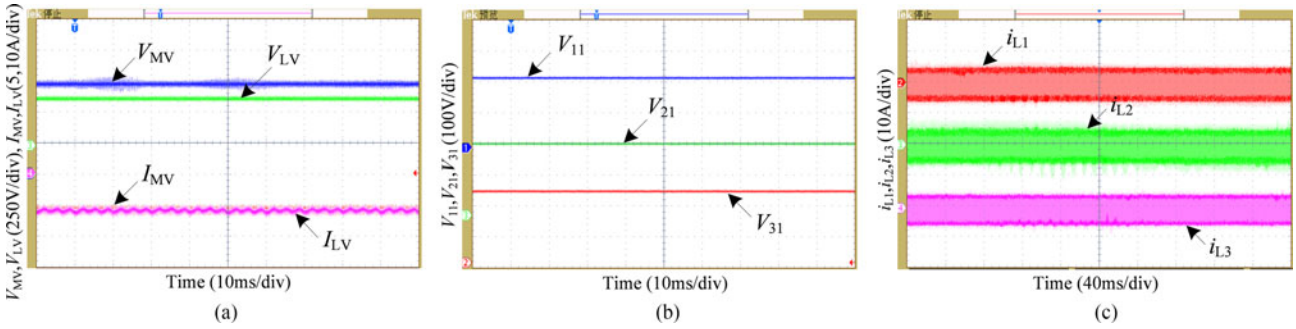

Fig. 24. Experimental results of steady operation for DCT in MVDC voltage control mode. (a) MVDC and LVDC voltage and current. (b) Series voltage. (c) HFL current.

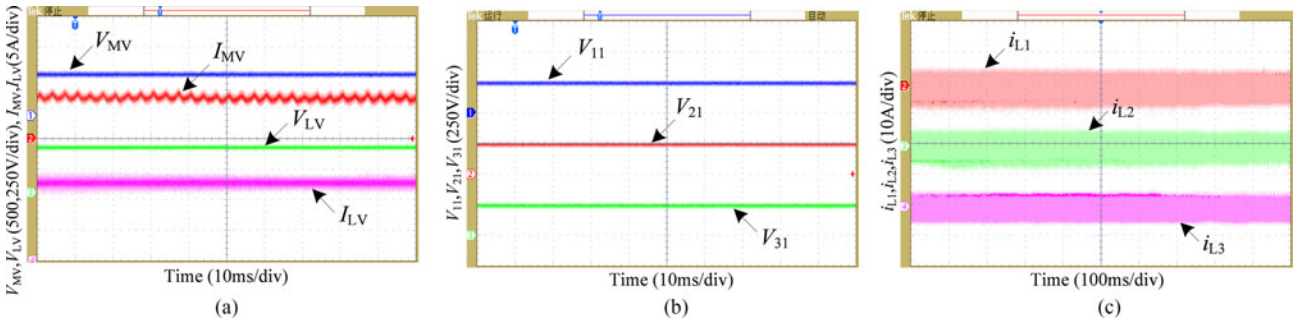

Fig. 25. Experimental results of steady operation for DCT in LVDC voltage control mode. (a) MVDC and LVDC voltage and current. (b) Series voltage. (c) HFL current.

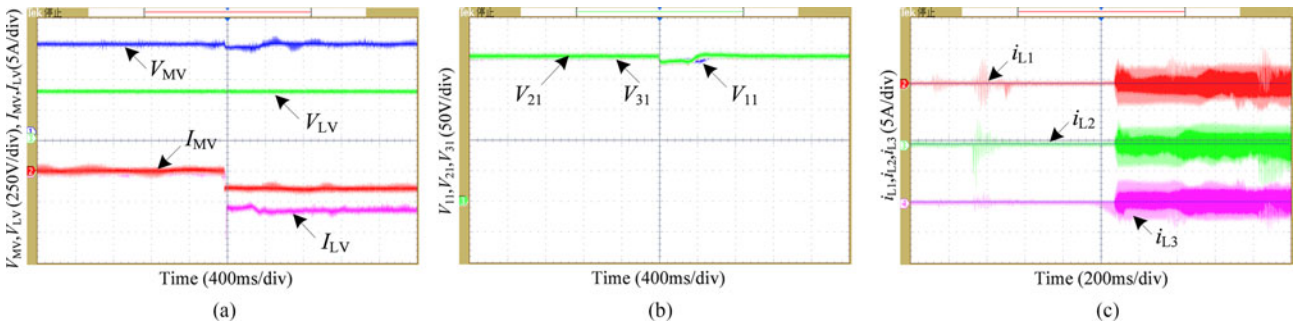

Fig. 26. Experimental results of transient operation for DCT in MVDC voltage control mode. (a) MVDC and LVDC voltage and current. (b) Series voltage. (c) HFL current.

control should be disabled. During steady process, all the driving pulses of switches are enabled and the balance control during operation process is enabled, the series voltages still keep balance.

D. Steady Operation Experiments

In the MVDC voltage control mode, the LVDC bus voltage is provided by external system, and the MVDC bus voltage is controlled by the DCT. The voltage and current waveforms of the MVDC and LVDC buses are shown in Fig. 24(a), and the voltage waveforms in the series side and the HFL current waveforms are shown in Fig. 24(b) and (c). It can be seen that the MVDC and LVDC buses remain at reference values steadily. Both the current and voltage conversions of the DCT operate normally. All the series voltages and HFL currents are equal, which reflects a good voltage and power balancing effect.

In the LVDC voltage control mode, the MVDC bus voltage is provided by MVDC distribution, and the LVDC bus voltage is controlled by the DCT. The experimental results are shown in Fig. 25. It can be seen that the power flow goes in the reverse direction, but performance of the DCT is also satisfactory and shows good voltage and power balancing effect.

In the power control mode, compared with LVDC voltage control mode, the unified reference I_{LVr} is directly calculated from a given reference, but not from LVDC voltage controller, the control is simpler, the waveforms are the same with that in the LVDC voltage control mode.

E. Transient Operation Experiments

When the power is changed in the MVDC voltage control mode, the experimental results of DCT are shown in Fig. 26. It can be seen that the LVDC bus remains nearly constant, the other

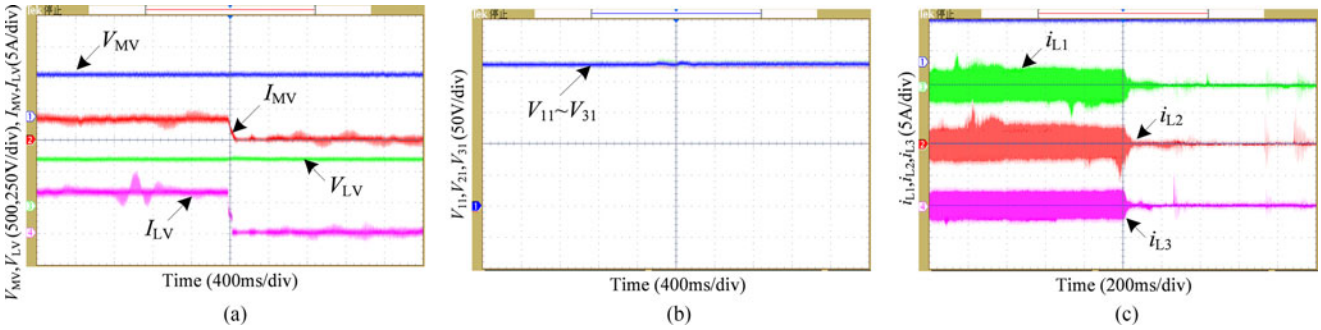

Fig. 27. Experimental results of transient operation for DCT in LVDC voltage control mode. (a) MVDC and LVDC voltage and current. (b) Series voltage. (c) HFL current.

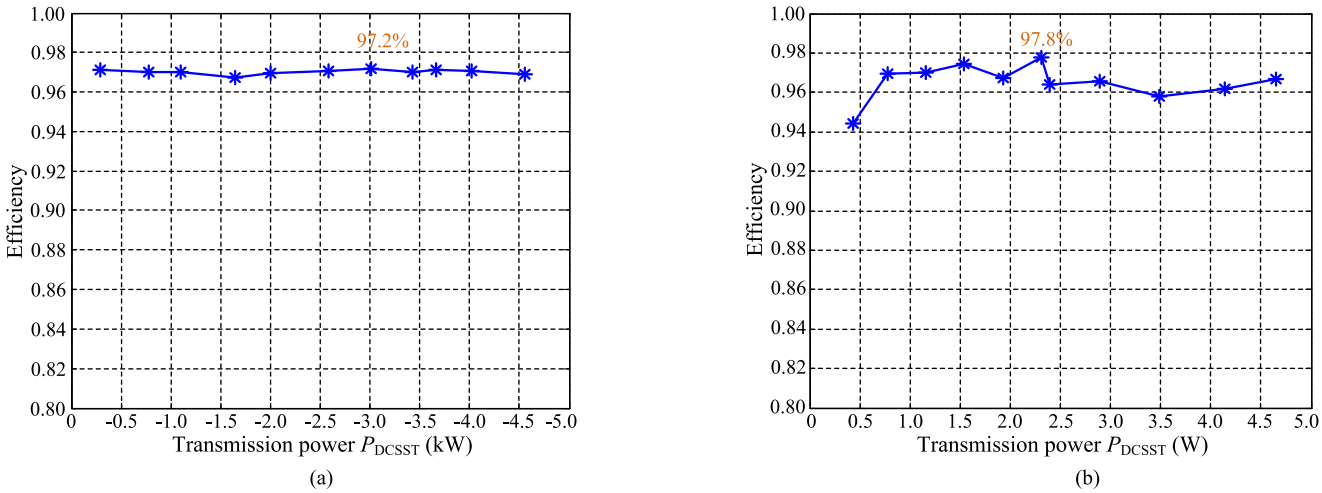

Fig. 28. Experimental results of efficiency varied with transmission power. (a) Reverse power flow. (b) Forward power flow.

voltages and currents are able to revert back to the steady state. Both a small overshoot and a short dynamic time are realized. After dynamic adjustment, the DCT still shows a fixed voltage and current conversion ratios, as well as good voltage and power balance.

The experimental results of the DCT when the power is changed in the LVDC voltage control mode are shown in Fig. 27. It can be seen that the MVDC bus remains nearly constant, and the DCT still shows a fixed voltage and current conversion ratios, as well as good voltage and power balances.

F. Efficiency Experiments

Fig. 28 shows the experimental results of the efficiency with a varying transmission power. When the power is transferred from the LVDC bus to the MVDC bus, the efficiencies of most ranges are above 96.0%, the efficiency at rated power $P_{\mathrm{DCSST}} = -4.5\,\mathrm{kW}$ is 96.9%, and the maximum efficiency of the DCT reaches up to 97.2%.When the power is transferred from the MVDC bus to the LVDC bus, the efficiencies of most ranges are above 96.0%, the efficiency at rated power $P_{\mathrm{DCSST}} = 4.5\,\mathrm{kW}$ is 96.7%, and the maximum efficiency reaches up to 97.8%. It needs to point out that the efficiency may changes with the change of the power, voltage and employed switches for every power electronics system, but the commutation behaviors for the same topology are the same; this means that although the specified values may be a little different, the efficiency for the same topology will have the similar regulation.

The efficiencies in Fig. 28(a) and (b) are measured in MVDC control and LVDC control modes, respectively. As mentioned in Section IV-C, in MVDC control mode, the series MVDC voltage is controlled by each DAB cell, the balancing controller is not needed, and the voltage and power balance in MVDC side can be achieved automatically. Thus, in the MVDC control mode, the series voltage has good stability. In the LVDC control mode, the additional balancing controller is added to adjust the series voltage, which cause a certain voltage ripple and HFL current ripple. Thus, the measured values has a certain ripple with the change of the power. In addition, the efficiencies in the paper are measured by the power meter YOKOGAWA WT230, the measurement accuracy can reach as high as 0.1%. The efficiency accounts for the loss of semiconductors and passive elements. From the earlier analysis, the performances of the DCT based on the proposed solution can satisfy the requirements of practical applications in MVDC distribution system, which has greater prospect, especially with the rapid development of VSC-HVDC transmission and LVDC microgrid.

X. Conclusion

The DCT will be the key device for MVDC power distribution. Comprehensive theoretical analysis and experimental verification for the practical application of DCT based on DAB in flexible MVDC distribution system are presented in the paper. Especially, the full-process operation modes, optimal modulation methods, full-process control strategy, fault-handling solution, design methods, and full-process experiments are analyzed and proposed. From the theoretical and experimental analysis, the optimal modulations can reduce the current stress during startup, steady and transient processes. The proposed control strategies can ensure the safe operation of DCT under MVDC control, LVDC control, and power control modes, especially ensure the voltage balance both during block and operation processes. The DCT based on the proposed solution not only achieves voltage conversion and electric isolation between the different dc buses but also actively controls voltage, current, and power between MVDC distribution grid and LVDC microgrid. The practical application of DCT in MVDC distribution are worth anticipating.

References

[1] S. M. Chen, T. J. Liang, and K. R. Hu, "Design, analysis, and implementation of solar power optimizer for dc distribution system," *IEEE Trans. Power Electron.*, vol. 28, no. 4, pp. 1764–1772, Apr. 2013.

[2] P. Peltoniemi, P. Nuutinen, and J. Pyrhonen, "Observer-based output voltage control for dc power distribution purposes," *IEEE Trans. Power Electron.*, vol. 28, no. 4, pp. 1914–1926, Apr. 2013.

[3] Y. C. Chang, C. L. Kuo, K. H. Sun, and T. C. Li, "Development and operational control of two-string maximum power point trackers in dc distribution systems," *IEEE Trans. Power Electron.*, vol. 28, no. 4, pp. 1852–1861, Apr. 2013.

[4] K. T. Mok, M. H. Wang, S. C. Tan, and S. Y. R. Hui, "DC electric springs-a technology for stabilizing dc power distribution systems," *IEEE Trans. Power Electron.*, vol. 32, no. 2, pp. 1088–1105, Feb. 2017.

[5] J. Lago and M. L. Heldwein, "Operation and control-oriented modeling of a power converter for current balancing and stability improvement of dc active distribution networks," *IEEE Trans. Power Electron.*, vol. 26, no. 3, pp. 877–885, Mar. 2011.

[6] H. Li, W. Li, M. Luo, A. Monti, and F. Ponci, "Design of smart MVDC power grid protection," *IEEE Trans. Instrum. Meas.*, vol. 60, no. 9, pp. 3035–3046, Sep. 2011.

[7] A. G. Exposito, J. M. Mauricio, and J. M. M. Ortega, "VSC-based MVDC railway electrification system," *IEEE Trans. Power Del.*, vol. 29, no. 1, pp. 422–431, Jan. 2014.

[8] N. Flourentzou, V. G. Agelidis, and G. D. Demetriades, "VSC-based HVDC power transmission systems: An overview," *IEEE Trans. Power Electron.*, vol. 24, no. 3, pp. 592–602, Mar. 2009.

[9] J. Beerten, S. Cole, and R. Belmans, "Modeling of multi-terminal VSC HVDC systems with distributed dc voltage control," *IEEE Trans. Power Syst.*, vol. 29, no. 1, pp. 34–42, Jan. 2014.

[10] S. Cui and S. K. Sul, "A comprehensive dc short circuit fault ride through strategy of hybrid modular multilevel converters (MMCs) for overhead line transmission," *IEEE Trans. Power Electron.*, vol. 31, no. 11, pp. 7780–7796, Nov. 2016.

[11] D. Jovcic and B. Teck, "Developing dc transmission networks using dc transformers," *IEEE Trans. Power Del.*, vol. 25, no. 4, pp. 2535–2543, Oct. 2010.

[12] N. Denniston, A. M. Massoud, S. Ahmed, and P. N. Enjeti, "Multiple-module high-gain high-voltage dc–dc transformers for offshore wind energy systems," *IEEE Trans. Ind. Electron.*, vol. 58, no. 5, pp. 1877–1886, May 2011.

[13] G. Buticchi and E. Lorenzani, "Detection method of the dc bias in distribution power transformer," *IEEE Trans. Ind. Electron.*, vol. 60, no. 8, pp. 3539–3549, Aug. 2013.

[14] B. Zhao, Q. Song, and W. Liu, "Efficiency characterization and optimization of isolated bidirectional dc–dc converter based on dual- phase-shift control for dc distribution application," *IEEE Trans. Power Electron.*, vol. 28, no. 4, pp. 1711–1727, Apr. 2013.

[15] B. Zhao, Q. Song, W. Liu, G. Liu, and Y. Zhao, "Universal high-frequency-link characterization and practical fundamental-optimal strategy for dual-active-bridge dc–dc converter under PWM plus phase-shift control," *IEEE Trans. Power Electron.*, vol. 30, no. 12, pp. 6488–6494, Dec. 2015.

[16] A. K. Rathore and U. R. Prasanna, "Analysis, design, and experimental results of novel snubberless bidirectional naturally clamped ZCS/ZVS current-fed half-bridge dc/dc converter for fuel cell vehicles," *IEEE Trans. Ind. Electron.*, vol. 60, no. 10, pp. 4482–4491, Oct. 2013.

[17] Y. W. Cho, W. J. Cha, J. M. Kwon, and B. H. Kwon, "High-efficiency bidirectional DAB inverter using a novel hybrid modulation for stand-alone power generating system with low input voltage," *IEEE Trans. Power Electron.*, vol. 31, no. 6, pp. 4138–4147, Jun. 2016.

[18] N. Hou, W. Song, and M. Wu, "Minimum-current-stress scheme of dual active bridge dc–dc converter with unified-phase-shift control," *IEEE Trans. Power Electron.*, vol. 31, no. 12, pp. 8552–8561, Dec. 2016.

[19] B. Zhao, Q. Song, W. Liu, and Y. Sun, "A synthetic discrete design methodology of high-frequency isolated bidirectional dc/dc converter for grid-connected battery energy storage system using advanced components," *IEEE Trans. Ind. Electron.*, vol. 61, no. 10, pp. 5402–5410, Jul. 2015.

[20] B. Zhao, Q. Song, W. Liu, and Y. Zhao, "Transient dc bias and current impact effects of high-frequency-isolated bidirectional dc–dc converter in practice," *IEEE Trans. Power Electron.*, vol. 31, no. 4, pp. 3203–3216, Apr. 2016.

[21] H. Behjati and A. Davoudi, "Power budgeting between diversified energy sources and loads using a multiple-input multiple-output dc–dc converter," *IEEE Trans. Ind. Appl.*, vol. 49, no. 6, pp. 2761–2772, Nov. 2013.

[22] P. Patra, J. Ghosh, and A. Patra, "Control scheme for reduced cross-regulation in single-inductor multiple-output dc–dc converters," *IEEE Trans. Ind. Electron.*, vol. 60, no. 11, pp. 5095–5104, Nov. 2013.

[23] H. Athab, A. Yazdani, and B. Wu, "A transformerless dc–dc converter with large voltage ratio for MV dc grids," *IEEE Trans. Power Del.*, vol. 29, no. 4, pp. 1877–1885, Apr. 2014.

[24] M. J. Carrizosa, A. Benchaib, P. Alou, and G. Damm, "DC transformer for dc/dc connection in HVDC network," in *Proc. 15th Eur. Power Electron. Appl.*, 2013, pp. 1–10.

[25] P. Zumel, L. Ortega, A. Lazaro, C. Fernandez, and A. Benchaib, "Control strategy for modular dual active bridge input series output parallel," in *Proc. 14h IEEE Workshop Control Modeling Power Electron.*, 2013, pp. 1–7.

[26] B. Zhao, Q. Song, W. Liu, and Y. Sun, "Overview of dual-active-bridge isolated bidirectional dc–dc converter for high-frequency-link power-conversion system," *IEEE Trans. Power Electron.*, vol. 29, no. 8, pp. 4091–4106, Aug. 2014.

[27] H. Qin and J. W. Kimball, "Closed-loop control of dc–dc dual-active-bridge converters driving single-phase inverters," *IEEE Trans. Power Electron.*, vol. 29, no. 2, pp. 1006–1017, Feb. 2014.

[28] B. Zhao, Q. Song, and W. Liu, "A practical solution of high-frequency-link bidirectional solid-state transformer based on advanced components in hybrid microgrid," *IEEE Trans. Ind. Electron.*, vol. 62, no. 7, pp. 4587–4597, Jul. 2015.

[29] H. Fan and H. Li, "A high-frequency medium-voltage converter for future electric energy delivery and management systems," in *Proc. 8th IEEE Int. Conf. Power Electron. ECCE Asia*, 2011, pp. 1031–1038.

[30] J. Li, B. Zhao, Q. Song, Y. Huang, and W. Liu, "Minimum voltage tracking balance control based on switched resistor for modular cascaded converter in MVDC distribution grid," *IEEE Trans. Ind. Electron.*, vol. 63, no. 9, pp. 5437–5441, Sep. 2016.

Biao Zhao (S'11−M'14) was born in Hubei, China, in 1987. He received the B.S. degree from the Department of Electrical Engineering, Dalian University of Technology, Dalian, China, in 2009, and the Ph.D. degree from the Department of Electrical Engineering, Tsinghua University, Beijing, China, in 2014.

He is currently a Postdoctoral Fellow in the Department of Electrical Engineering, Tsinghua University. His current research interests include high-power dc–dc converters, power electronic transformers, and flexible dc transmission and distribution systems.

Dr. Zhao is a member of the IEEE Power Electronics Society, the Industrial Electronics Society, and the Chinese Society for Electrical Engineering.

Qiang Song (M'14) was born in Changchun, China, in 1975. He received the B.S. and Ph.D. degrees from the Department of Electrical Engineering, Tsinghua University, Beijing, China, in 1998 and 2003, respectively.

He is currently an Associate Professor in the Department of Electrical Engineering, Tsinghua University. His current research interests include high-power electronic interfaces for utility systems, flexible ac transmission systems, and motor drives.

Jianguo Li was born in Hebei, China, in 1975. He received the B.S. degree from the Department of Electrical Engineering, North China Electric Power University, Baoding, China, in 1997, and the M.S. degree from the Department of Electrical Engineering, Tsinghua University, Beijing, China, in 2005. He is currently working toward the Ph.D. degree in electrical engineering at the North China Electric Power University, Beijing.

His current research interests include bidirectional dc–dc converters, high-frequency-link power conversion systems, and flexible dc transmission and distribution systems.

Qianhao Sun was born in Shanxi, China, in 1993. He received the B.S. degree from the Department of Electrical Engineering, Northeast Electric Power University, Jilin, China, in 2014. He is currently working toward the M.S. degree in the Department of Electrical Engineering, Tsinghua University, Beijing, China.

His current research interests include high-power dc–dc converters and flexible dc transmission and distribution systems.

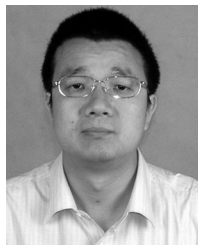

Wenhua Liu was born in Hunan, China, in 1968. He received the B.S., M.S., and Ph.D. degrees from the Department of Electrical Engineering, Tsinghua University, Beijing, China, in 1988, 1993, and 1996, respectively.

He is currently a Professor in the Department of Electrical Engineering, Tsinghua University. His current research interests include high-power electronic and flexible ac transmission systems.